Design and Optimization of a New Magnetic-Geared Pole-Changing Hybrid Excitation Machine

Xing Zhao, and Shuangxia Niu *IEEE member*

The Hong Kong Polytechnic University, Department of Electrical Engineering, Kowloon, Hong Kong

***Abstract*— This paper presents a new magnetic-geared pole-changing hybrid excitation machine (MG-PCHEM), which can provide high torque density and improved flux weakening ability. The key is to flexibly change the pole pair number of inner excitation sources by injecting variable dc field currents, and hence regulate the dominant pole-pair flux components to realize an effective magnetic field adjustment. In the following paper, the machine configuration and its operation principle of flux control are introduced firstly. Then, the influences of some leading design parameters are analyzed including the slot pole combination and other dimension parameters, and after which a comparative study is carried out with the traditional single-stator topology. Based on the optimal alternative, electromagnetic performance of the MG-PCHEM is further evaluated by using finite element method (FEM). Finally, a prototype is designed, manufactured and fully tested. Relevant experimental results verify the feasibility of this new hybrid solution as well as the finite-element predictions.**

***Index Terms*— Hybrid excitation machine, magnetic-geared, magnetic field adjustment, pole-changing.**

I. Introduction

PERMANENT magnet (PM) magnetic gear (MG) has been paid much attention in the recent years since it can offer the advantages such as high torque transmission capability, reduced acoustic noise and overload protection. A typical MG has been proposed as shown in Fig. 1(a), in which a modulation layer is creatively embedded into two separate PM rotors, which are named as the high-speed less-pole rotor and low-speed multi-pole rotor, respectively. By introducing such a modulation layer composed with steel segments, a transmitted torque density exceeding 100 kNm / m^3 is reported to be achieved [1-2]. Another type of MG has also been investigated in [3], as shown in Fig. 1(b), in which the high-speed rotor is made as a spoke-type structure instead of the surface-mounted type, and by doing so, relatively higher air-gap flux density can be obtained and less consideration needs to be given to the manufacturing difficulty and centrifugal forces for the PMs.

In the recent years, inspired by the magnetic-gearing effect in MGs, a number of magnetic-geared machines (MGM) have been proposed in the literature, aimed at eliminating the gearbox in conventional machine systems. In [4-5], a PM brushless machine is artfully integrated into a MG so that they can share a common PM rotor, and hence the low-speed requirement for direct driving and the high-speed requirement for compact machine design can be achieved simultaneously. In [6], by replacing the high-speed PM rotor in a MG with the stationary armature windings, a new MGM is proposed for direct-drive applications. In the abovementioned MGMs, the PMs are all located in the rotating component. Nevertheless, over the past two years, another kind of MGM, namely partitioned-stator machines (PSMs) has also been widely studied [7-8], in which the PMs and armature windings are placed in the inner and outer stator, respectively, and the modulation layer acts as an output component. These so-called PSMs are actually developed from conventional stator-PM machines such as flux switching machines (FSMs) or flux reversal machines (FRMs) [9-10], but they can also be regard as a kind of MGMs considering their internal magnetic-gearing effect [11]. These existed MGMs have already shown some potential for the low-speed direct drive applications. Nevertheless, in some variable-speed applications such as electric vehicle and wind power generation, not only the low-speed high-torque ability, but also the flux weakening ability and a corresponding wide constant power range are desired.

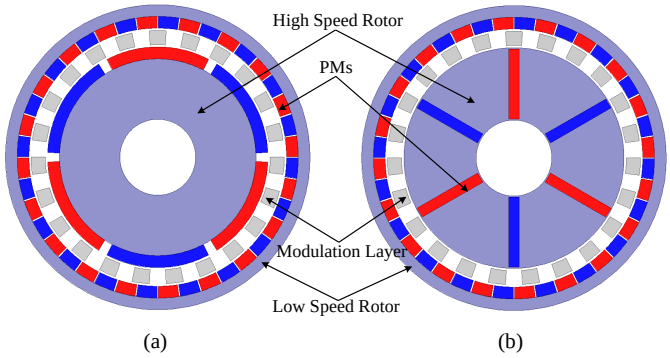

Fig. 1. Two typical magnetic gears. (a) Surface-mounted-type magnetic gears (b) Spoke-type magnetic gears

Hybrid excitation machines (HEM), which employs both PM and field excitation, have been widely investigated due to their distinct flux weakening ability [12-14]. From the perspective of magnetic circuits, HEMs can be divided into two typical groups, namely series hybrid excitation machine (SHEM) and parallel hybrid excitation machine (PHEM), respectively. SHEMs possess a significant advantage of the simple and compact structure. However, the field flux has to pass through the PMs and due to its low permeability, the reluctance of the field magnetic path is quite high, and thus a large ampere-turn field potential is needed to interact with PM excitation, leading to the relatively lower efficiency for magnetic field adjustment. Besides, the system reliability in SHEMs will be inevitably reduced since there is a risk of

demagnetization. As for the PHEMs, the PM excitation and field excitation have independent flux trajectories, and in other words, the flux created by field coils does not pass through the PMs, which leads to an improved field adjustment ability and zero demagnetization risk.

Introducing the hybrid excitation into MGMs could provide a potential solution for variable-speed direct-drive applications. One of the important design considerations for the HEMs is how to realize the brushless configuration, and from this perspective, among all the mentioned MGMs, the partitioned-stator topology is the most suitable one to introduce field excitation, since all their PMs are located in the stationary body and no brush or slip rings is needed for the field current regulation. Some partitioned-stator hybrid topologies have been investigated in the literature, including both the series [15] and parallel [16] topologies. These existed topologies make a meaningful exploration in the hybrid solutions for variable-speed applications

Another important concept, namely pole-changing, is also developed for the flux weakening operation in the hybrid PM machines, in which traditionally Al-Ni-Co magnetic material with low coercive force is adopted independently or combined with NdFeB magnetic material, and the pole-changing flux weakening effect can be achieved by injecting short current pulse into the magnetizing winding. Basically, there are two kinds of pole-changing PM machines proposed in literature, AC excited [17] and DC excited topologies [18]. However, some common problems exist in different PCPM topologies which limit their practical applications, such as, how to realize an accuracy control of the Al-Ni-Co magnetization level and meanwhile avoid the demagnetization risk [19].

This paper aims to integrate abovementioned two popular concepts in a spoke-type MGM, which has the parallel hybrid magnetic circuits and pole-changing capability, respectively. A new magnetic-geared pole-changing hybrid excitation machine, namely MG-PCHEM, is proposed and implemented for the first time, which may provide good torque density, improved pole-changing flux weakening capacity as well as zero demagnetization risk at the same time. This paper is organized as following. In the section II, the configuration of MG-PCHEM and its operating principle of pole-changing flux control will be illustrated firstly. Then in section III, the influences of some leading design parameters will be analyzed and optimized, after which a comparative study will be carried with the existed single-stator topology. Based on the optimal design, the electromagnetic performance of MG-PCHEM will be further evaluated in section IV, by using the finite element analysis (FEA). In section V, a prototype is manufactured and tested. Relevant experimental results will be given to verify the feasibility of the new machine topology. Finally, some conclusions will be drawn in section VI.

II. Machine Configuration and Operation Principle

A. Machine configuration

Fig.2 shows the configuration of the proposed MG-PCHEM, which comprises two separate stators and a sandwiched modulation rotor. The outer stator consists of steel laminations and a single-layer non-overlapping armature winding. The modulation rotor consists of evenly distributed nonmagnetic and magnetic steel segments. The inner stator is made as a spoke type structure which mainly includes steel laminations, PMs and concentrated field coils. All the PMs are tangentially magnetized and adjacent PMs have opposite magnetization directions as illustrated by the arrows. Similarly, adjacent field coils also have opposite polarities and all these field coils are connected in series to form a single field excitation and interact with PM excitation. Some merits are integrated with this new hybrid topology. Firstly, a brushless structure is achieved for the field current regulation since the field winding is located in the inner static body. Secondly, the double stator structure can significantly enhance the space utilization ratio since all the field coils, PMs and armature windings have no space conflict with each other. Lastly, the spoke-type PM excitation in the inner stator gives a higher air-gap flux density due to flux-concentrating effect, and further benefiting from inherent magnetic gearing effect, this machine can achieve an improved torque density.

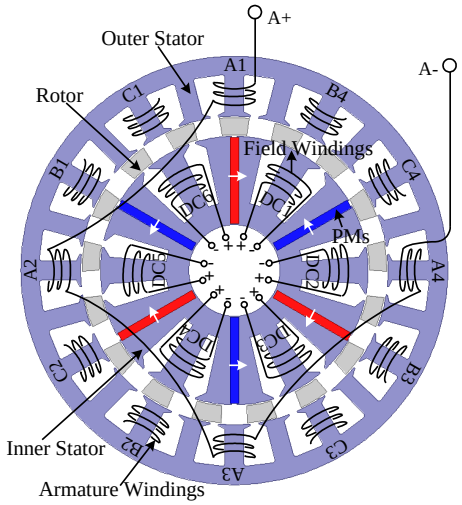

Fig. 2. Proposed magnetic-geared hybrid excitation machine.

Due to the existence of modulation steel segments, the magnetic field produced by two excitation sources in the inner stator is no longer uniform. Instead, a large number of magnetic harmonic components will be produced and their pole pair number (PPN) can be obtained from [1]

$$PPN_{m,k} = |mp_s + kp_r| \qquad m = 1,3,5\ldots, k = 0,1,2,3\ldots \tag{1}$$

where p_s is the PPN of the inner excitation sources, p_r is the number of modulation steel segments.

The corresponding rotational velocities of each harmonic component are [1]

$$\omega_{m,k} = \frac{kp_r}{mp_s + kp_r}\omega_r \tag{2}$$

where ω_r is the rotational velocity of the modulation rotor.

With the modulation effect by steel segments, harmonics with the same pole pair number and same rotational speed as those of the armature field will be produced and interact with each other. And to get the highest transmitted electromagnetic torque, the number of modulation steel segments, the PPN of the inner excitation sources, and the PPN of the armature

windings, are governed by [6] [11]

$$p_r = p_s + p_a \tag{3}$$

where p_a is the PPN of outer armature windings. And the magnetic gearing ratio in the proposed machine can be expressed as

$$G_r = \frac{p_a}{p_s} \tag{4}$$

B. *Pole-changing flux weakening operation*

Fig. 3 shows the operation principle of pole-changing flux weakening operation in the proposed machine. When only PM excitation is active, the flux distribution is shown in Fig. 3(a). It shows six tangential magnetized PMs comprise a 6-pole magnetic field, and the effective flux starts from the inner PMs, then passing through the modulation rotor to interact with armature windings in the outer stator, and finally comes back to the PMs again. When there is only field excitation, the corresponding flux distribution is presented in Fig. 3(b). One can see the effective flux starts from the inner wounded poles, then shorted by the modulation rotor and comes back through the adjacent iron cores. It is obvious this flux loop doesn't pass through the PMs, thus belonging to a parallel magnetic circuit. Besides, the pole number of the field excitation is 18 (denoted in the form of NSNSNS), instead of 6 compared to that of the PM excitation (NNNSSS). It can be seen this pole number difference is mainly caused by the opposite polarities of the inner wounded poles during flux weakening operation.

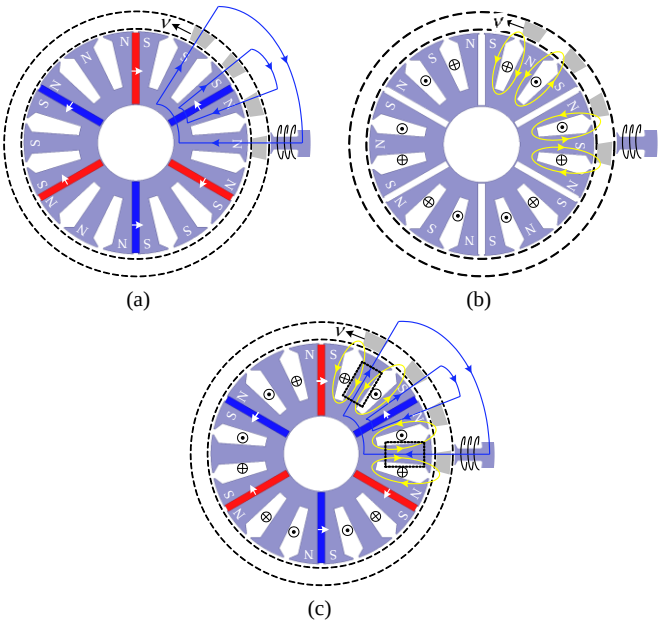

Fig. 3. Schematic flux distribution during pole-changing. (a) Only PMs. (b) Only field excitation. (c) PMs with field excitation.

Therefore, when these two excitation sources are combined together as shown in Fig. 3(c), polarities of the inner wounded poles become uncertain, as highlighted by the dash box, which are actually dependent on the magnetomotive force ratio between the PM and field excitation. In other words, by applying different field current, the polarity of inner wounded poles can be flexibly changed, thus so-called pole-changing operation can be realized in the inner excitation stator, and then the dominant flux harmonic components in the outer air gap can be further regulated to effectively adjust the armature flux, after the modulation effect of steel segments. Meanwhile, benefiting from the parallel magnetic circuit, there will be no demagnetization risk during the pole-changing operation.

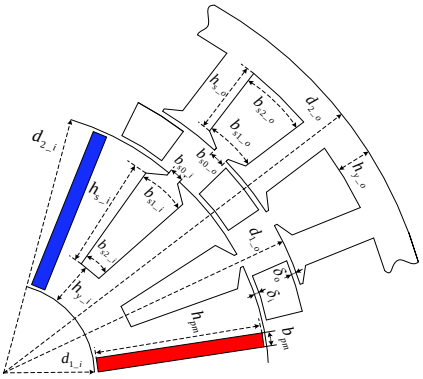

Fig. 4. Some general dimension parameters of MG-PCHEM.

TABLE I
General dimension parameters of MG-PCHEMs

Symbol	Parameter	Value
d_{2_o}	outer diameter of outer stator	150 mm
d_{2_i}	inner diameter of outer stator	108 mm
d_{1_o}	outer diameter of inner stator	94 mm
d_{1_i}	inner diameter of inner stator	32 mm
l	stack length	80 mm
δ_o	outer air-gap length	0.5 mm
δ_i	inner air-gap length	0.5 mm
b_{s2_o}	bottom width of outer slots	11 mm
b_{s1_o}	top width of outer slots	8 mm
b_{s0_o}	open width of outer slots	3 mm
h_{s_o}	height of outer slots	14 mm
h_{y_o}	height of outer yoke	5 mm
b_{s2_i}	bottom width of inner slots	4 mm
b_{s1_i}	top width of outer slots	8.5 mm
b_{s0_i}	open width of inner slots	2.5 mm
h_{s_i}	height of inner slots	23 mm
h_{y_i}	height of inner yoke	6 mm
b_{pm}	width of PMs	3 mm
h_{pm}	height of PMs	29.5 mm

TABLE II
Materials and specifications

	Parameters	value
PMs	Material	NdFeB35
	Remanence	1.2 T
	Coercive force	915 kA/m
Steels	Material	DW310_35
	Saturated flux density	2.0 T
	Mass density	7650 kg/m^3

III. DESIGN OPTIMIZATION AND COMPARATIVE STUDY

A. *Slot pole combination*

To design a new machine, it is essential to find a proper slot pole combination firstly. In this paper, an analytical and FEA combined method is adopted to find the optimal combination.

Some general design parameters are determined based on the following consideration. Firstly, the number of PMs in the inner stator should be relatively small to reserve enough space

for the introduction of field excitation. In the proposed design, the pole number of inner PMs is fixed at 6. Then, to create a multi-pole armature field, the number of outer slots is more suitable to be larger and fixed at 24 in this paper.

The number of the modulation steel segments (MSS) is a relatively flexible design variable in MG-PCHEMs, and once it is determined, the pole-pair number of the outer armature windings will also be determined by (3). And the winding electrical frequency of the MG-PCHEMs is governed by

$$f = \frac{N \times P_r}{60} (Hz) \tag{5}$$

where N is the rated speed and P_r is the number of MSSs. From this equation, one can see that different from traditional rotor-PM machines, the winding electrical frequency of the proposed MG-PCHEM is governed by the machine speed and MSS number, rather than the pole number of PMs. And in general, higher electrical frequency at rated speed gives higher torque density. Therefore, to enhance the power density and reduce the machine volume, relatively higher number of MSSs is analytically adopted for comparison. Meanwhile, taking the winding factor into consideration, FEA models of the proposed MG-PCHEM with MSS number changing from 11 to 19, will be separately built and compared.

Strictly speaking, all the dimension parameters should be optimized independently with each slot pole combination for a fair torque density comparison. However, considering the slot pole combination is recognized to be the most leading design variable in MGMs [20], a simplified comparison is adopted in this process to save optimization time, in which all the models share common design parameters apart from the MSS number and corresponding armature winding configurations. Some general dimension parameters are labeled in Fig. 4, with their detailed values listed in Table I. The average electromagnetic torque with 6A armature current under only PM excitation, is regarded as the common criterion for comparison.

TABLE III
Comparison with different pole-pair combinations

Number of steel segments	PPN of armature windings	Torque (Nm)	Winding factor
11	8	3.2	0.866
12	9	-	-
13	10	3.8	0.966
14	11	4.3	0.958
15	12	-	-
16	13	4.7	0.958
17	14	5.2	0.966
18	15	-	-
19	16	3.4	0.866

The FEA results with different slot pole combinations are listed in Table III. It can be seen, when the MSS number changes from 11 to 19, there are three cases can't work. Specifically, with 15 MSSs, the pole-pair number of armature windings needs to be 12, and in that case, the 24 slot and 12 pole combination can't create a three-phase machine but a single-phase one. Apart from that, cases with 12 and 18 MSSs present asymmetry back EMF, thus are not taken into consideration. Among all the feasible cases, it is apparent that the case with 17 MSSs and corresponding 14 pole-pair armature windings shows the largest torque density as well as the best winding utilization ratio. Therefore, the MG-PCHEM with 17 MSSs is selected as an optimal alternative.

B. Dimension parameters

Once the slot pole combination is selected, corresponding dimension parameters should be further optimized to improve the machine performance. For instance, the open slot width affects the cogging torque and back EMF harmonics; the stator tooth width affect the slot area for armature winding as well as inner saturation; etc. All these parameters have a coupled and comprehensive influence on the machine torque performance. Some dimension parameters in double stators to be optimized can be selected from Table I based on the existed conclusions [21], apart from that, due to the special rotor structure in the proposed topology, three additional rotor parameters are also determined in this paper, as illustrated in Fig. 5, which are the inner central angle of MSS, outer central angle of MSS, and its height, denoted as θ_{s2} , θ_{s1} , h_s , respectively.

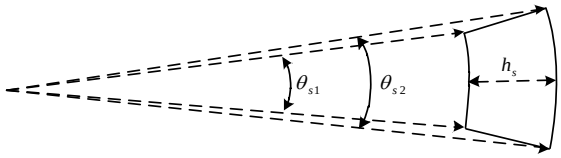

Fig. 5. Dimension parameters of steel segments.

TABLE IV
Selected parameters, variation ranges and optimized values

	Parameters	Lower limit	Upper limit	Optimized
Outer stator	b_{s0_o}	2.5 mm	3.5 mm	2.8 mm
	b_{s2_o}	10.5 mm	13.5 mm	11.3 mm
	h_{y_o}	4.5 mm	6.3 mm	4.7 mm
Inner stator	b_{s0_i}	2.5 mm	3.5 mm	3.1 mm
	b_{s2_i}	3.5 mm	5.5 mm	4.6 mm
	h_{y_i}	5.5 mm	7.5 mm	6.3 mm
Rotor	h_s	13.5 mm	19.5 mm	14.3 mm
	θ_{s1}	4.5°	6.5°	5.1°
	θ_{s2}	4.5°	6.5°	5.7°

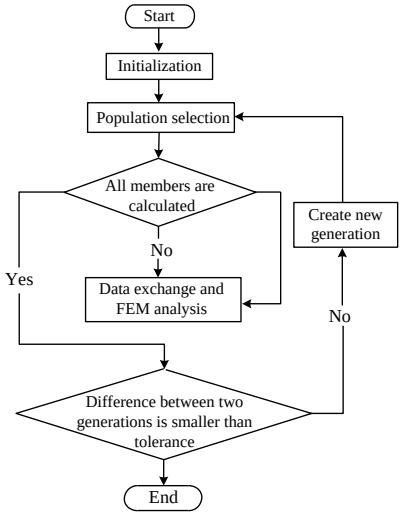

Fig. 6. Flowchart of the coupled FEA and GA optimization

Due to the complexity of magnetic field distribution, it is difficult to optimize these dimension parameters by traditional

analytical method. Therefore, in this paper, an intelligent algorithm is introduced, namely genetic algorithm (GA). GA has three operation factors, namely, reproduction, crossover and mutation. Reproduction generates the most adaptive individual survival, when crossover and mutation are responsible for expanding the searching scope. In such a way, GA can find the optimal solution by imitating the effect of natural selection [22]. Further, a coupled optimization between FEA and GA is used to optimize these dimension parameters. To realize this coupled analysis, an intelligent script is established based on the C language for data communication between the Maxwell (a FEA software) and the Visual Studio (a programming software). Its flow chart is presented in Fig. 6. This coupled FEA and GA method can dramatically cut off the time consumption since no manual adjustment is needed.

Relatively higher average torque and lower torque ripple value are pursued as the main objectives of the optimization. The optimization is processed with following considerations: a population of 30 elements, the maximum generation number of 25, crossover probability of 0.7, and mutation probability of 0.1. Fig. 7 presents the optimized result of each element in the last generation. It is found that some elements have relatively lower torque ripple but also lower average torque, while some other elements have higher average torque but also higher torque ripple. These unsuitable cases are natural products of a multi-objective optimization. A few elements are artificially selected as highlighted by the dash circle, which have both acceptable torque ripple and torque density. The optimization parameters and their final design values are all listed in Table IV. Fig. 8 shows steady torque waveforms with original and optimized design parameters. One can see, with FEA and GA combined optimization, the average torque of MG-PCHEM is enhanced by 19% and its torque ripple is decreased by 58%.

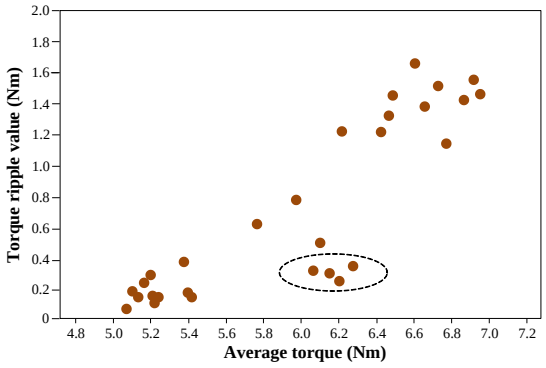

Fig. 7. Element values of last generation.

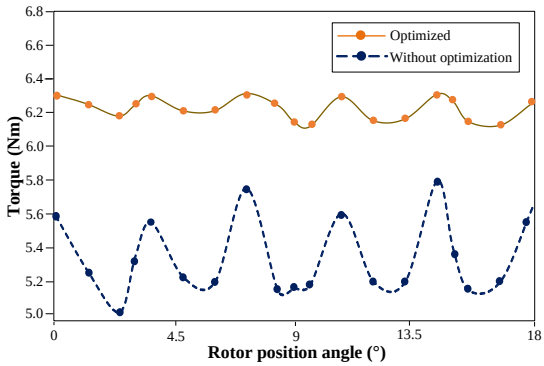

Fig. 8. Electromagnetic torque waveforms.

TABLE V
Comparison between MG-PCHEM and existed single-stator HEM

Parameters	Proposed MG-PCHEM	Traditional single-stator HEM
Outer diameter	150 mm	150 mm
Axial length	80 mm	80 mm
Air gap length	0.5 mm	0.5 mm
PM usage	43200 mm^3	43200 mm^3
Slot space-factor	0.6	0.6
Current density	6 A/mm^2	6 A/mm^2
Phase voltage	44 V	36 V
Average torque	6.2 Nm	5.1 Nm

C. Comparison with single-stator structure.

To verify the advantage of this novel double-stator HEM, a quantitative comparison is carried out between the proposed MG-PCHEM and the traditional single-stator HEM [12]. Two models share some common design parameters including the outer diameter, axial length, air gap length, and so on as listed in the Table V. It can be seen the calculated torque of MG-PCHEM is 21% larger than that of the single-stator HEM. An explanation for this phenomenon is inherent magnetic gearing effect in the MG-PCHEM. Specifically, the modulation layer in MG-PCHEM brings about rich higher-order magnetic field harmonics which has faster rotational speed that in the single-stator HEM, accordingly, the proposed machine has enhanced working frequency and improved torque density.

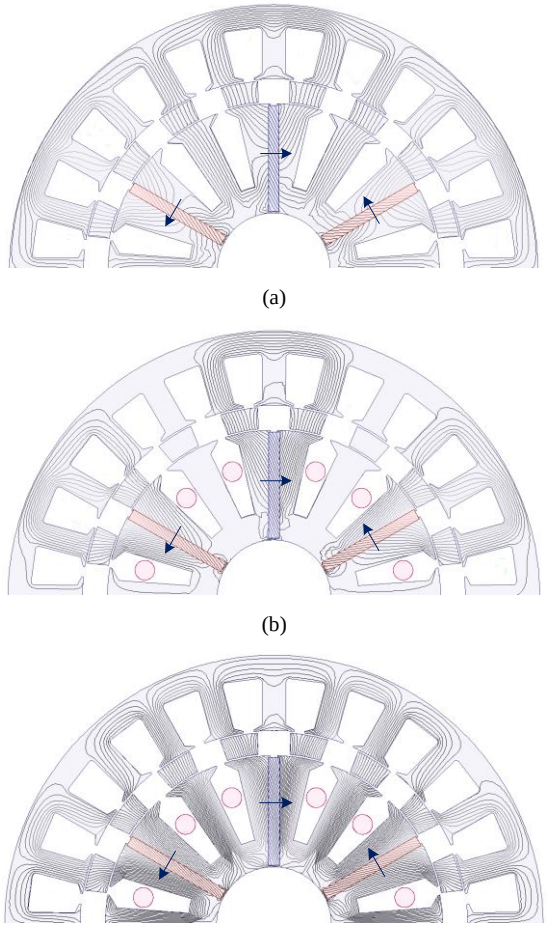

(a)

(b)

(c)

Fig. 9. No load magnetic field distribution during pole changing. (a) Only PM excitation. (b) PMs with 6A field current. (c) PMs with 12A field current.

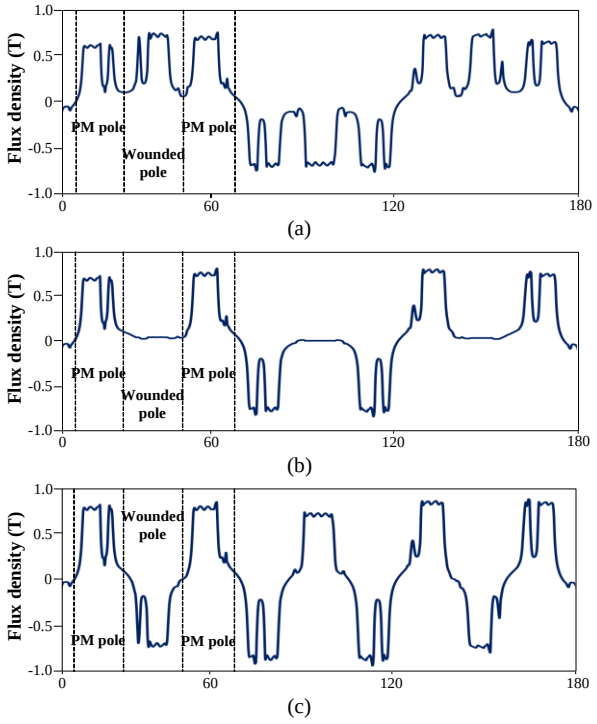

Fig. 10. Outer air gap flux density during pole changing. (a) Only PM excitation. (b) PM with 6A field current. (c) PM with 12A field current.

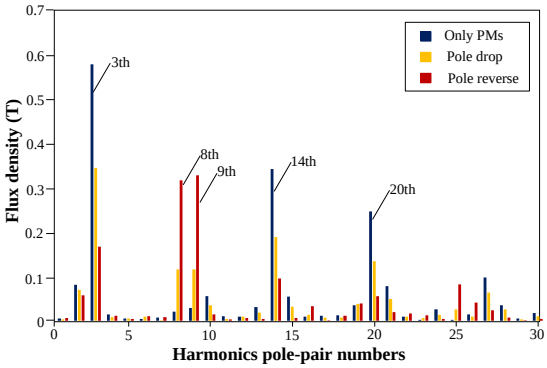

Fig. 11. FFT analysis of the pole changing results in outer air gap.

IV. Electromagnetic Performance Analysis

Based on the optimization results, the modulation rotor uses 17 steel segments, accordingly, a 14-PPN single-layer non-overlapping armature winding is adopted as shown in Fig. 2, which has the merits of simpler wire wrap, eliminated layer insulation and thus higher slot space-factor, compared with a double-layer configuration [23]. After that, the performance of this new MG-PCHEM is further evaluated by using FEA.

A. Magnetic field distribution during pole changing

The magnetic field distribution at different excitation status is calculated and plotted in Fig. 9. One can see, with different field current applied, the inner stator changes its excitation status effectively, and correspondingly, distinct pole-changing phenomenon of the flux distribution in the outer stator can be observed. To clearly investigate the magnetic field variation, the flux density in outer air gap is calculated which directly interacts with the armature windings, as shown in the Fig. 10. According to the relative positions with excitation sources, the flux density waveform can be divided into two parts, namely wounded poles and PM poles, respectively, as denoted by the dash lines. One can see, when there is only PM excitation, the wounded and PM poles share the same polarities and similar amplitudes, about 0.6T as shown in the Fig. 9(a). And when 6A field current is applied, flux density of the wounded poles almost drop to zero as shown in the Fig. 9(b), while the PM poles present a little increase to 0.7T. Then, when 12A field current is injected, the wounded pole reverses its polarity to negative 0.7T and the PM poles continuously increase to 0.8T as in Fig. 9(c). Hence, by applying different field excitation, the inner wounded pole can flexibly change its polarity, thus realize so-called pole-changing operation. Meanwhile, one can see during this wounded-pole-changing operation, flux density of the PM poles presents a continuous but relatively modest growth, which indirectly proves that no demagnetization risk exists in the proposed MG-PCHEM.

By using the Fourier analysis, the harmonics components of the flux density in the outer air gap is deduced and plotted in Fig. 11. One can see, when there is only PM excitation, the dominant harmonic components in the outer air gap are the 3th, 14th and 20th, respectively. These dominant components will interact with the armature field and generate electromagnetic torque effectively. When the pole-drop occurs by applying negative field excitation, amplitudes of those original dominant harmonics almost all decrease to half, and meanwhile, other order components come out, especially the 8th and 9th one. Then, when the pole-reverse phenomenon occurs, the original main harmonics almost decrease to zero, while the 8th and 9th one becomes dominant components, as a result, highly flux-weakening operation is achieved.

The different pole-pair numbers of two excitation sources in the inner stator, lead to this asymmetric harmonic distribution at different excitation status. As analyzed in Section II, the pole number of the field excitation is 18 instead of 6 compared with that of the PM excitation. As a result, when the field excitation is enhanced, the proportion of 8^{th} and 9^{th} harmonic components will both increase in the outer air gap after the modulation effect by 17 steel segments. In other words, this pole changing operation can effectively regulate the dominant harmonics distribution to realize flux weakening operation.

B. Flux linkage variation

Further, the flux linkage variation of a single-phase winding is presented in Fig. 12. One can see that highly sinusoidal waveforms are achieved, which means this machine is more suitable for brushless AC operation. Besides, the armature flux linkage can be effectively adjusted and little distortion or phase shifting is observed during flux regulation, thus proving the feasibility of the proposed design.

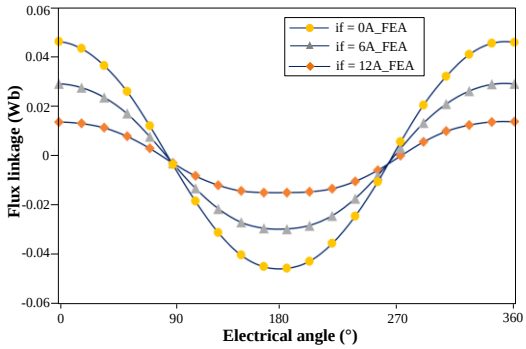

Fig. 12. Flux linkage of A phase winding.

C. *Steady torque performance*

Fig. 13 shows the calculated steady torque by injecting 6A sinusoidal armature current. It can be seen the electromagnetic torque can be steadily regulated by different field current. An approximate 21% torque ripple ratio is observed during highly flux weakening, which is relatively larger than that with only PM excitation. However, in general, the torque performance is acceptable during a wide range of field regulation.

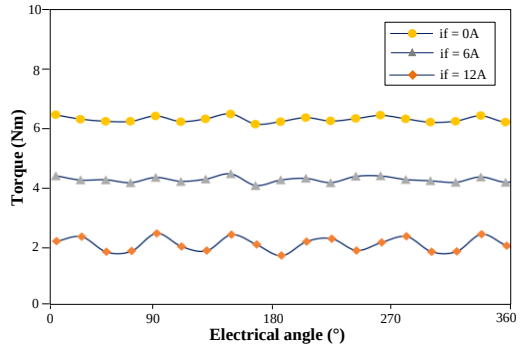

Fig. 13. Steady torque with 6A armature current injection.

(a) (b) (c)

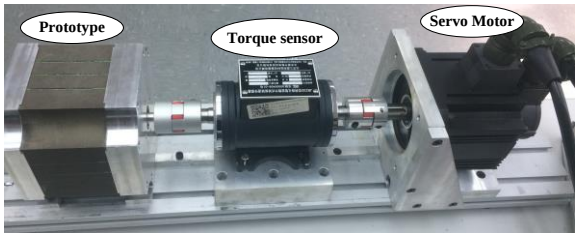

(d)

Fig. 14. Prototype. (a) Outer stator. (b) Inner stator. (c) Rotor. (d) Test bed

V. EXPERIMENT VARIATION

To verify the feasibility of the proposed hybrid solution, a machine prototype is manufactured with relevant parameters listed in Table I. The key components are shown in Fig. 14, which includes an outer stator, an inner stator and a sliced rotor, respectively. As shown in Fig. 14(a), the outer stator is composed of steel laminations and single-layer concentrated armature windings. Fig. 14(b) shows the inner stator which mainly consists of the steel laminations, six tangentially magnetized PMs and six concentrated field coils. The rotor structure is relatively special, and considering the mechanical strength requirement, it is not made up of steel laminations, instead, discrete steel bars are adopted and then fixed by lock screw and two end plates, forming a complete rotor as shown in Fig. 14(c), with which the shaft is linked. These three components are assembled together, and a test bed is further established as shown in Fig. 14(d), which mainly includes this prototype, a torque sensor and a servo machine.

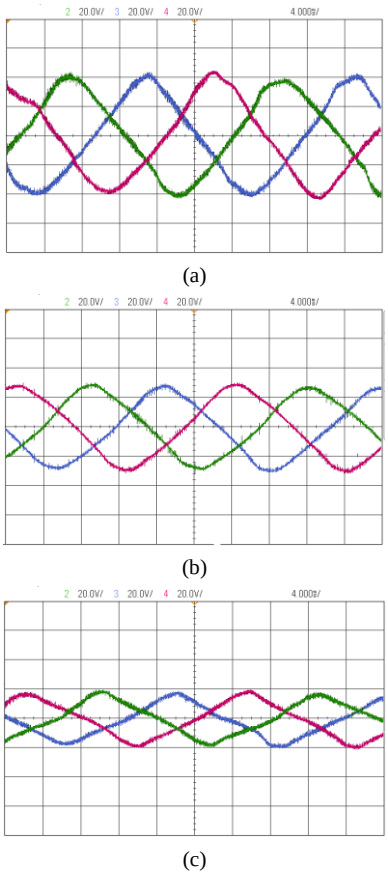

(a) (b) (c)

Fig. 15. Measured no load back EMF with different field current. (a) Only PM excitation. (b) PM and 6A field current. (c) PM and 10A field current.

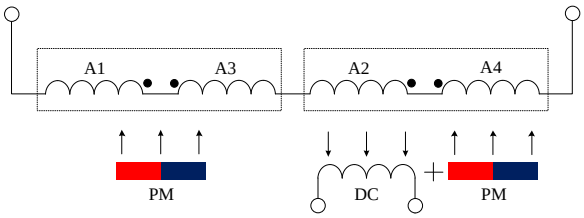

Fig. 16. Alignment between the armature coils and inner excitation sources.

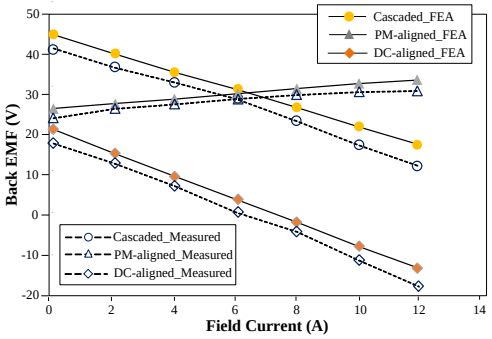

Fig. 17. Measured and FEA predicted back EMF-field current curve.

A. *Back EMF test*

The back EMF of three phase windings are measured and presented in Fig. 15, at speed 600 rpm. It can be seen the induced voltage can be effectively regulated by injecting different field current. To more clearly investigate the status of excitation sources, a winding-splitting test is further carried out. As shown in Fig. 2, a single-phase winding is composed

of four separate coils, taking phase A as an example, it consists of coil A1, A2, A3 and A4, respectively. According their relative positions with the inner excitation sources, these four coils can be divided into two groups as denoted in Fig. 16. A1 and A3 are aligned with the PM poles, thus are named as PM-aligned part, while A2 and A4 are aligned with the wounded poles, thus named as DC-aligned part. The measured voltage curves of these two parts are presented in Fig. 17, with field current varying from 0A to 12A. One can see, the PM-aligned part shows less voltage variation, while DC-aligned part shows a much larger variation range which changes from positive 19V to negative 18V. Hence, when these two parts are cascaded together, an adjustable synthetic voltage can be obtained. This winding-splitting test indirectly proves the ability of wounded-pole-changing flux control as the FEA predicted. The existed difference between the measured values and FEA predicted results, is mainly caused by the prototype fabrication tolerance, such as an uneven magnetization of PM material as well as a tolerance in the airgap length.

B. *Torque capacity test*

The torque-angle curve is tested and presented in the Fig. 18, by injecting a constant dc current into the armature winding and fixing the rotor at different positions. The output torque can be steadily regulated and no distinct reluctance torque component is observed. Then, the envelope curve of the peak torque is presented in Fig. 19, it can be found when the armature current increases from 6A to 17A, the output torque accordingly increases from 6.5N to 17.5N, and after which a saturation phenomenon occurs. Therefore, approximate three-times overload ability and peak power can be achieved if a corresponding cooling condition is provided to increase the current density.

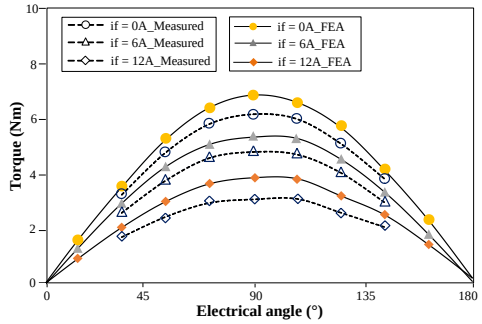

Fig. 18. Torque characteristics against electrical angle.

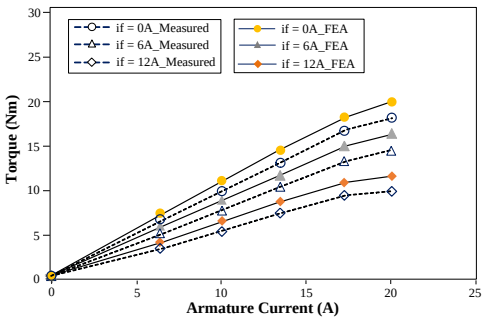

Fig. 19. Measured torque-armature current curve at different excitation status.

C. *Torque speed test*

Fig. 20 presents the measured torque-speed curves under different field excitation, with the limit of 140V dc bus voltage. The base speed of the proposed machine when there is no field current, is set at 600 rpm. It is obvious that by applying the field excitation, flux weakening operation can be achieved, which results in a higher base speed as well as higher output torque in the higher speed region, compared to that with only PM excitation, although the base speed increase is relatively limited due to the armature reaction. In general, an extended constant power range can be obtained in this prototype.

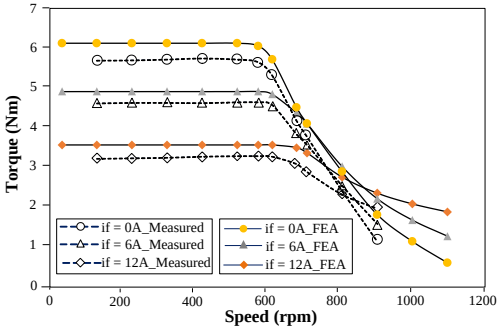

Fig. 20. Measured torque-speed curves at different excitation status

D. *Power, loss and efficiency test*

The machine efficiency η is defined as

$$\eta = \frac{p_o}{p_m + p_f} \tag{6}$$

where p_o, p_m, p_f is the output mechanical power, input electrical power from the power source, as well as the input electrical power fed to the field terminals which is also known as the field copper loss, respectively. It can be seen, when only PM excitation is active, the machine efficiency can reach 87%. Further, when a field current is applied for flux weakening, the machine accordingly enters a constant power region and the output mechanical power maintains at about 385W. With field loss increasing, the machine efficiency inevitably decreases to 56% when highly flux weakening occurs. However, in general, the efficiency can be maintained above 60% over a wide range of field current regulation.

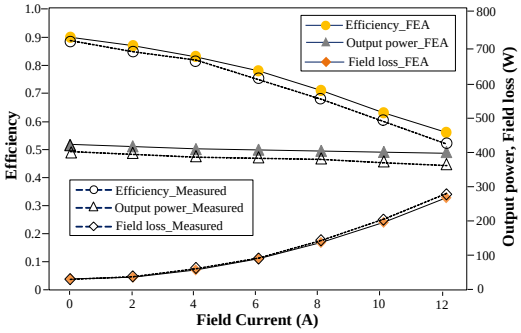

Fig. 21. Output power, field loss and efficiency.

VI. CONCLUSION

Due to the good torque density, magnetic-geared machine (MGM) has been a potential solution for some direct-drive applications. To further develop a flux-controllable MGM for

the variable-speed applications, this paper presents a novel magnetic-geared pole-changing hybrid excitation machine, namely MG-PCHEM. The machine structure and its operation principle of pole-changing flux control, are firstly introduced. Then, some leading design parameters, including the slot pole combination and some dimension parameters, are discussed and optimized. Further, based on the optimal design, the pole-changing flux weakening ability of MG-PCHEM is verified by using finite element analysis (FEA). Finally, a prototype is manufactured and tested, relevant experiment results verify the feasibility of the proposed topology and FEA predictions. In general, the main merits of MG-PCHEM are summarized as improved torque density, brushless structure, pole-changing flux-weakening ability as well as zero demagnetization risk. Whereas, unilateral magnetic force exists in this design case, meanwhile, the machine complexity and cost should be further reduced by simplifying its structural design and mechanical processing technologies, especially for the special modulation rotor, which will be considered in the following-up research

REFERENCES

[1] K. Atallah, D. Howe, "A novel high-performance magnetic gear", *IEEE Trans. Magn.*, vol. 37, no. 4, pp. 2844-2846, Jul. 2001.

[2] S. Niu, N. N. Chen, S. L. Ho, and W. N. Fu, "Design optimization of magnetic gears using mesh adjustable finite element algorithm for improved torque," *IEEE Trans. Magn.*, vol.48, no. 11, pp.4156-4159, Nov. 2012.

[3] P. O. Rasmussen, T. O. Andersen, F. T. Jorgensen, O. Nielsen, "Development of a high-performance magnetic gear", *IEEE Trans. Ind. Appl.*, vol. 41, no. 3, pp. 764-770, May/Jun. 2005.

[4] K. T. Chau, D. Zhang, J. Z. Jiang, C. Liu "Design of a magnetic-geared outer-rotor permanent-magnetic brushless motor for electric vehicles", *IEEE Trans. Magn.*, vol. 43, no. 6, pp. 2504-2506, Jun. 2007.

[5] Y. Liu, S. Niu, and W.N. Fu, "Design of an electrical continuously variable transmission based wind energy conversion system," *IEEE Transactions on Industrial Electronics*, vol.PP, no.99, pp.1-1. 2016.

[6] L. L. Wang, J. X. Shen, P. C. K. Luk, W. Z. Fei, C. F. Wang, H. Hao, "Development of a magnetic-geared permanent-magnet brushless motor", *IEEE Trans. Magn.*, vol. 45, no. 10, pp. 4578-4581, Oct. 2009.

[7] D. J. Evans, and Z. Q. Zhu, "Novel partitioned stator switched flux permanent magnet machines," *IEEE Trans. Magn.*, vol. 51, no. 1, Jan. 2015.

[8] Z. Z. Wu, Z. Q. Zhu and H. L. Zhan, "Comparative Analysis of Partitioned Stator Flux Reversal PM Machines Having Fractional-Slot Nonoverlapping and Integer-Slot Overlapping Windings," *IEEE Trans. Energy Convers*, vol. 31, no. 2, pp. 776-788, June 2016.

[9] K. T. Chau, C. C. Chan, C. Liu, "Overview of permanent-magnet brushless drives for electric and hybrid electric vehicles", *IEEE Trans. Ind. Electron.*, vol. 55, no. 6, pp. 2246-2257, Jun. 2008.

[10] M. Cheng, W. Hua, J. Zhang, W. Zhao, "Overview of stator-permanent magnet brushless machines", *IEEE Trans. Ind. Electron.*, vol. 58, no. 11, pp. 5087-5101, Nov. 2011.

[11] Z. Wu and Z. Zhu, "Analysis of Magnetic Gearing Effect in Partitioned Stator Switched Flux PM Machines," *IEEE Trans. Energy Convers*, vol. 99, no. 1, pp. 1-1, Oct, 2016.

[12] Q.S. Wang and S. Niu, "Overview of flux-controllable machines: Electrically excited machines, hybrid excited machines and memory machines", *Renewable and Sustainable Energy Reviews*, vol. 68, pp.475-491, 2017.

[13] J. A. Tapia, F. Leonardi, and T. A. Lipo, "Consequent-pole permanent magnet machine with extended field-weakening capability," *IEEE Trans. Ind. Appl.*, vol. 39, no. 6, pp. 1704–1709, Dec. 2003.

[14] O. Laldin, S.D. Sudhoff and S. Pekarek, "Analysis and design of hybrid machines for DC generation," *IEEE Trans. Energy Convers*, vol. 30, no. 3, pp. 1192-1199, Sept. 2015.

[15] H. Hua, Z. Q. Zhu, and H.L. Zhan, "Novel consequent-pole hybrid excited machine with separated excitation stator," *IEEE Trans. Ind. Electron.*, vol. 63, no.8, pp. 4718-4728, Aug.2016.

[16] H. Hua and Z. Q. Zhu, "Novel parallel hybrid excited machines with separate stators," *IEEE Trans. Energy Convers*, vol. 31, no. 3, pp. 1212-1220, Sept. 2016.

[17] V. Ostovic, "Pole-changing permanent-magnet machines," *IEEE Transactions on Industry Applications*, vol. 38, no. 6, pp. 1493-1499, Nov/Dec 2002.

[18] F. Li, K. T. Chau, C. Liu and C. Qiu, "New approach for pole-changing with dual-memory machine," *IEEE Trans. Appl. Supercond.*, vol. 24, no. 3, pp. 1-4, June 2014.

[19] F. Li, K. T. Chau and C. Liu, "Pole-Changing Flux-Weakening DC-Excited Dual-Memory Machines for Electric Vehicles," *IEEE Trans. Energy Convers*, vol. 31, no. 1, pp. 27-36, March 2016.

[20] S. Wang, W. Zhao, J. Ji, L. Xu and J. Zheng, "Magnetic Gear Ratio Effects on Performances of Linear Primary Permanent Magnet Vernier Motor," IEEE Trans. Appl. Supercond., vol. 26, no. 7, pp. 1-5, Oct. 2016.

[21] L. Wu, R. Qu, D. Li, Y. Gao, "Influence of pole ratio and winding pole numbers on performances and optimal design parameters of surface permanent magnet Vernier machines", *IEEE Trans. Ind. Appl.*, vol. 51, no. 5, pp. 3707-3715, Sep./Oct. 2015.

[22] K. J. Han, D. H. Cho, and H. K. Jung, "Optimal core shape design for cogging torque reduction of BLDC motor using genetic algorithm," *Proc. Compumag.*, Sapporo, Japan, 1999, pp. 332–333.

[23] J. H. J. Potgieter and M. J. Kamper, "Torque and voltage quality in design optimization of low-cost non-overlap single layer winding permanent magnet wind generator," *IEEE Trans. Ind. Electron*, vol. 59, no. 5, pp. 2147-2156, May, 2012.

Xing Zhao received the B.Sc. degree from the Department of Automation at Nanjing University of Aeronautics and Astronautics, China, in 2014, and currently he is pursuing a Ph.D. degree in the department of electrical engineering at the Hong Kong Polytechnic University, Hong Kong. His research interests include the design and control of novel electric machines for the EV/HEV and renewable energy systems.

Shuangxia Niu received the B.Sc. and M.Sc. degrees in electrical engineering from the School of Electrical Engineering and Automation, Tianjin University, Tianjin, China, in 2002 and 2005, respectively, and the Ph.D. degree in electrical engineering from the Department of Electrical and Electronic Engineering, The University of Hong Kong, Hong Kong, in 2009. Since 2009, she has been with The Hong Kong Polytechnic University, Kowloon, Hong Kong, where she is currently an Assistant Professor in the Department of Electrical Engineering. She has authored or coauthored over 70 papers in leading journals. Her research interests include the design and control of novel electrical machines and drives, renewable energy conversion systems, and applied electromagnetics.